

RSC Advances



This is an *Accepted Manuscript*, which has been through the Royal Society of Chemistry peer review process and has been accepted for publication.

Accepted Manuscripts are published online shortly after acceptance, before technical editing, formatting and proof reading. Using this free service, authors can make their results available to the community, in citable form, before we publish the edited article. This *Accepted Manuscript* will be replaced by the edited, formatted and paginated article as soon as this is available.

You can find more information about *Accepted Manuscripts* in the [Information for Authors](#).

Please note that technical editing may introduce minor changes to the text and/or graphics, which may alter content. The journal's standard [Terms & Conditions](#) and the [Ethical guidelines](#) still apply. In no event shall the Royal Society of Chemistry be held responsible for any errors or omissions in this *Accepted Manuscript* or any consequences arising from the use of any information it contains.

COMMUNICATION

Hydrofluoric Acid-induced Fluorination and Formation of Silica Nanocapsules for ^{19}F Magnetic Resonance Imaging

Cite this: DOI: 10.1039/x0xx00000x

Received 00th January 2012,
Accepted 00th January 2012Luís M. F. Lopes^a and Laura M. Ilharco^{a†}

DOI: 10.1039/x0xx00000x

www.rsc.org/

A new, easy and economical method for producing fluorinated hollow silica nanoparticles using an aqueous hydrofluoric acid solution is reported, and a physico-chemical insight is proposed.

Fluorine-based compounds and materials have found application in a large number of technological domains and gave rise to a very active research field, mostly due to their outstanding, and sometimes unexpected, properties.^[1,2] However, harmful methods of fluorination and expensive fluorinated precursors have wrecked their acceptance as practical widespread solutions.

Since, in general, fluorine-based materials are regarded as chemically inert under most biological conditions, a wide range of biomedical applications has been intended, from diagnosis and therapeutic nanocarriers to permanent implants.^[3-6]

Given fluorine's biological rarity and its strong intrinsic magnetic signal, the fluorinated compounds and materials labelled with the naturally abundant ^{19}F -isotope have gained relevance on the biomedical imaging field, replacing the classical heavy metals^[7] as contrast agents for Magnetic Resonance Imaging (MRI),^[8,9] whereas tracer molecules labelled with the radioactive ^{18}F -isotope have been used in Positron Emission Tomography (PET).^[10,11] Both technologies have emerged as powerful, non-invasive, *in vivo* imaging tools in oncology, neurology, psychiatry and cardiology.^[12]

In recent years, special attention has been driven towards approaches using fluorinated nanoparticles, mostly silica- and polymer-based, designed for diagnostic imaging tools combined with drug delivery capabilities.^[13,14] Taking into consideration the biocompatibility, chemical stability and structural control of silica materials *versus* polymeric matrices, the former tend to be preferred.

Most fluorinated silica nanoparticles found in the literature are obtained either by a sol-gel process involving the condensation of perfluoroalkyl di- or tri-alkoxysilanes,^[15] or by surface functionalization of preformed silica nanoparticles with perfluoroalkyl alkoxysilanes^[16,17] or fluoropolymers.^[18] In some cases, such surface modification results in the improvement of the nanoparticles' solubility, stability and dispersion in different solvents.^[19] More particular approaches of fluorination have been

applied to silica-based materials other than nanoparticles, namely the direct F_2 functionalization,^[20] the synthesis with hydrofluoric acid (HF)^[21] or fluoride-containing salts (*e.g.* KF, NaF, NaBF_4 or NH_4F), which lead to the formation of $[\text{SiF}_6]^{2-}$ octahedral species,^[22] to fluorine chemisorption and hydroxyls replacement.^[23] Other methods include reactive ion etching involving CF_4 ,^[24] as well as plasma enhanced chemical vapour deposition (PECVD) with SF_6 , CF_4 , C_2F_6 , SiF_4 or HF.^[25,26]

In the present work, hollow silica nanoparticles with average external diameter (ϕ_{TEM}) of 37 ± 9 nm and with large empty nanocages (Fig. 1A) were obtained by combination of the reverse emulsion method (a mixture of cyclohexane, triton X-100, hexanol and HF aqueous solution) with the sol-gel reactions of tetraethoxysilane (TEOS), and subsequent functionalization with 3-aminopropyl-trimethoxysilane (APTS), used in order to increase the particles' stability in biological media. Under these conditions, the silica network formed only at the interface between the aqueous and the cyclohexane phases. From the SEM micrograph (Fig. 1B) it becomes clear that these particles, although not perfectly spherical, exhibit a three-dimensional morphology and a considerable degree of association. This is a drastic change in comparison to the typical morphology of silica nanoparticles prepared by the exact same procedure, but using water instead of HF solution (Fig. 1C): these are larger, spherical, bulk silica nanoparticles with average diameter (ϕ_{TEM}) of 57 ± 5 nm.

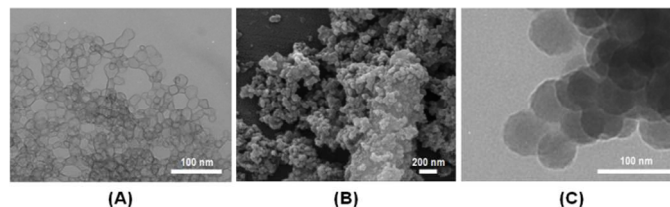


Figure 1: TEM (A) and SEM (B) micrographs of silica nanocapsules fluorinated with a 4%wt HF aqueous solution. For comparison, a TEM micrograph (C) of bulk silica nanoparticles produced by the same procedure, using water instead of HF solution.

The diffuse reflectance infrared Fourier transform (DRIFT) spectrum of these silica nanocapsules (Fig. 2) evidences the efficiency of HF as fluorinating agent: the very strong band at 746 cm^{-1} is assigned to the $\nu\text{Si-F}$ mode in $\text{O}_{4/2}\text{SiF}$ species with intermediate geometry between tetrahedral and octahedral, or to the $\nu\text{Si-O-Si}$ mode of relaxed bonds due to the occurrence of strongly polarized Si-F bonds in their vicinity.^[20] It is so strong that it masks the $\nu\text{sSi-O-Si}$ band expected at $\sim 800\text{ cm}^{-1}$. An additional band related to fluorinated species appears at 991 cm^{-1} , assigned to the $\nu\text{sSi-F}$ modes of $\text{O}_{2/2}\text{SiF}_2$ and $\text{O}_{1/2}\text{SiF}_3$ tetrahedral species,^[23] but it is partially overlapped with the stronger $\nu_{\text{as}}\text{Si-O-Si}$ band, centred at 1066 cm^{-1} (Fig. 2B). The weak $\nu\text{Si-OH}/\nu\text{Si-O}^-$ band at 937 cm^{-1} reveals a low content of uncondensed silanol groups or broken siloxane bridges. It attests the inefficiency of the silica network condensation, confirmed by the low intensity of the νOH broad band centred at $\sim 3150\text{ cm}^{-1}$, assigned to hydrogen bonded hydroxyl groups. Only very few free hydroxyl groups are present, responsible for the very weak component at higher wavenumber (3615 cm^{-1} , Fig. 2C).

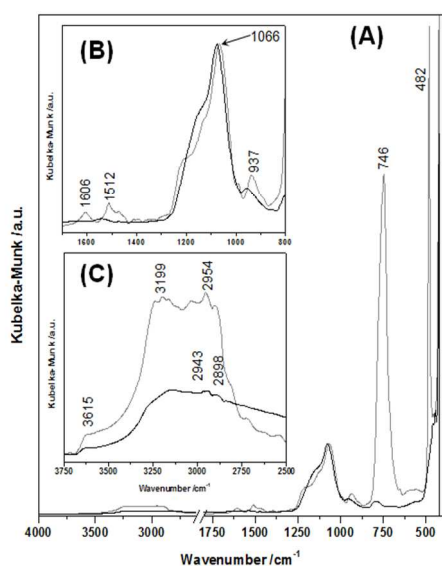


Figure 2: (A) - DRIFT spectra of fluorinated silica nanocapsules ($\text{SiO}_2\text{-F}$, gray line) and of non-fluorinated bulk silica nanoparticle (SiO_2 , black line). The spectra were normalized to the $\nu_{\text{as}}\text{Si-O-Si}$ band ($1066/1076\text{ cm}^{-1}$). (B) and (C) - two enhanced regions.

The spectral comparison in Fig. 2 shows that, in the bulk nanoparticles resulting from the same synthesis in the absence of HF, condensation is even more efficient: the bands related to silanol groups are weaker relatively to the main silica band. Besides, the maximum of the $\nu_{\text{as}}\text{Si-O-Si}$ band is shifted to 1076 cm^{-1} and its profile quite distinct. We may correlate these differences to the reaction mechanism and kinetics that give rise to different silica structures. When the aqueous phase within the Triton X-100 micelles is acidified by HF, any TEOS molecules that migrate to the interface are rapidly hydrolyzed and condensed under the catalytic effect of HF, resulting in a silica spherical crown near the interface. When the aqueous phase is neutral, hydrolysis occurs more slowly and only after the addition of ammonia, by a basic mechanism. Under these conditions, the silica nucleation process prevails and the silica network develops extending to all the micelle cavity, resulting in bulk nanoparticles.^[27] The silica structure will be readdressed below, in a more quantitative treatment.

The other features in the spectra of Fig. 2 could be assigned to the surface modifier (APTS), since residual Triton X-100 was

removed by a repeated washing procedure. The contribution of APTS bands to the bulk nanoparticles spectrum is not significant, which is not surprising given the much higher relative amount of silica network. The series of weak bands above 3000 cm^{-1} , overlapped with the broad and very weak $\nu\text{O-H}$ band (Fig. 2C), is assigned to νNH_2 modes of APTS, involved in hydrogen bonds with other amine or hydroxyl groups of neighbour particles. The corresponding scissors mode appears at 1606 and 1512 cm^{-1} (Fig. 2B). These bands confirm the amine functionalization by the surface modifier, and the different hydrogen bonding interactions between silanol and/or surface amine groups of neighbour particles. The ρCH_3 mode of APTS (which appears as a very strong band at $\sim 817\text{ cm}^{-1}$ in the spectrum of the pure compound) is absent, showing that the methoxy groups of APTS have been hydrolyzed. The proposed band assignments are summarized in Table S1 (ESI).

The interparticle interactions suggested by the DRIFT spectra may justify the association effect observed on the TEM and SEM micrographs (Fig. 1), and has been corroborated by dynamic light scattering (DLS) measurements in deionised water. In fact, for the bulk nanoparticles, a bimodal size distribution was obtained with average diameters of 74 ± 9 and $161\pm 18\text{ nm}$, corresponding to the hydrodynamic diameters of the individual particles and of aggregates, respectively; in contrast, for the nanocapsules, only a broad single distribution was obtained, with average dimension of $507\pm 24\text{ nm}$, which shows a higher degree of aggregation. The fluorinated nanocapsules and their interactions are schematically represented in Fig. 3.

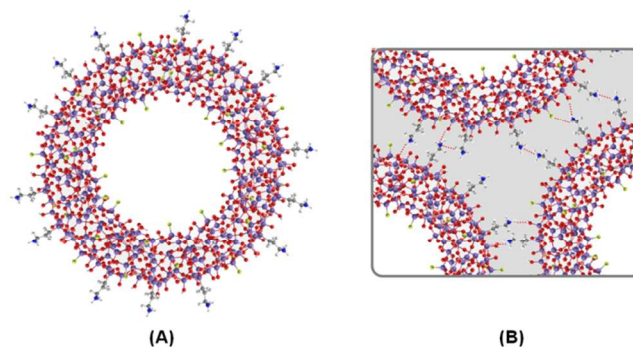


Figure 3: Schematic representation of a fluorinated silica nanocapsule (A) and the interparticle interactions responsible for its association (B). Color code: purple - Si; red - O; gray - C; light gray - H; blue - N; green - F.

The potential of HF as fluorinating agent was used in a different strategy, consisting in the *post*-synthesis fluorination of the bulk silica nanoparticles described above. Although the silica dissolution by this acidic source was expected, the results were surprising. Analyzing the differences between the TEM images of these particles before (Fig. 4B) and after (4C) addition of an 8%wt HF solution, it becomes clear that partial silica destruction of the nanoparticles was promoted by HF, rendering rough surfaces. However, similarly to the observed for the fluorinated hollow silica nanoparticles, this process was accompanied by introduction of fluorine atoms in the silica network, as proved by the appearance of the $\nu\text{Si-F}$ band at 741 cm^{-1} in the DRIFT spectrum (Fig. 4A) and by the detection of fluorine (at $\sim 0.7\text{ keV}$) in the EDS spectrum (Fig. 4D).

The breaking of some siloxane bridges induced by the silica dissolution process gives rise to an increase in the number of silanol groups, shown in the DRIFT spectrum by the enhanced relative intensities of the $\nu\text{Si-OH}/\nu\text{Si-O}^-$ (at 955 cm^{-1}) and $\nu\text{O-H}$ bands. The broadening of the characteristic $\nu_{\text{as}}\text{Si-O-Si}$ band suggests structural

modifications of the silica structure. The proposed band assignments of the DRIFT spectra of these silica particles are also included in Table S1.

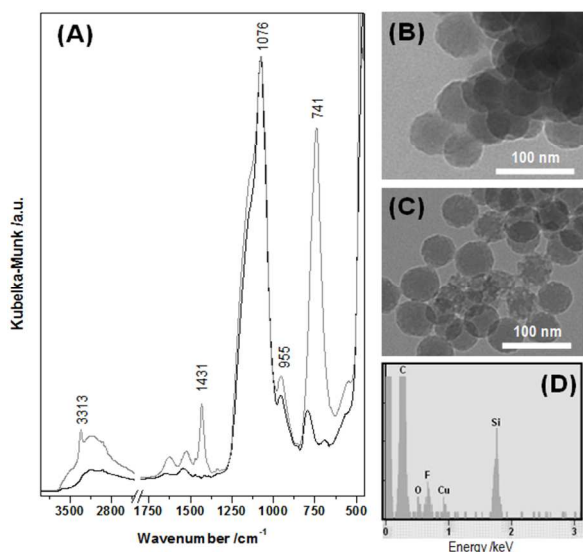


Figure 4: (A) - Comparison between the DRIFT spectra of bulk (SiO_2 , black line) and *post-synthesis* HF fluorinated (SiO_2 -*postF*, gray line) silica nanoparticles, normalized to the $\nu_{\text{asSi-O-Si}}$ band; TEM image of bulk SiO_2 (B) and of SiO_2 -*postF* (C) nanoparticles; EDS spectrum of SiO_2 -*postF* (D).

The silica structure was quantitatively analyzed by deconvolution of the $\nu_{\text{asSi-O-Si}}$ band (860 - 1300 cm^{-1}) in a sum of Gaussian components. The relevant results are summarized in Table 1.

Table 1. Results of deconvolution of the DRIFT spectra of the different silica nanoparticles in the 860 - 1300 cm^{-1} region, using a non-linear least squares fitting method (peak fitting module of OriginPro 7.0). The best fits were obtained with $\chi^2 \approx 10^{-5}$ and correlation coefficient of 0.9999 .

Sample	Wavenumber / cm^{-1}										ω_{CH_2} % (SiO_6)*		
	$\nu\text{Si-OH/O}^-$		$\nu\text{Si-F}$		$\nu_{\text{asSi-O-Si}}$								
	TO_6	LO_4	TO_6	LO_4	TO_6	TO_4	LO_4	LO_6			(APTS)		
SiO_2	903 (0.5)	951 (5.9)	-	-	1066 (42.8)	1076 (8.9)	1150 (37.2)	1210 (4.7)			-	51	
SiO_2 -F	899 (1.4)	937 (6.3)	991 (2.5)	-	1030 (5.7)	1064 (37.4)	1127 (31.1)	1229 (4.8)	1197 (10.8)			-	13
SiO_2 - <i>postF</i>	920 (2.6)	959 (5.8)	995 (0.7)	-	1067 (43.4)	1078 (0.9)	1149 (40.4)	1212 (6.2)			-	55	

Relative areas in % - between brackets. TO_6 (or TO_4) and LO_6 (or LO_4) correspond to the transverse and longitudinal optic components of the six (or four) membered siloxane rings (SiO_6 (or SiO_4)).

*%(SiO_6) = $100 \times [A(\text{TO}_6) + A(\text{LO}_6)] / A(\nu_{\text{asSi-O-Si}})$.

These results were interpreted taking into account that the elementary SiO_4 units of the silica network are mostly arranged in four-membered (SiO_4) and six-membered (SiO_6) siloxane rings, reflected in the spectra by partially overlapped bands corresponding to the $\nu_{\text{asSi-O-Si}}$ mode of each type of cycle, and, in each case, split into a pair of longitudinal optic (LO)/transverse optic (TO) components.^[28] The relative areas of these components (Table 1) confirm that the fluorinated silica nanocapsules have a completely different silica structure from the bulk particles. In the nanocapsules there is a large predominance of four-fold siloxane rings (87%) and a large splitting between the optic components of the six-fold rings (199 cm^{-1}), suggesting a more porous silica structure. Additionally, a component at 1197 cm^{-1} was clearly retrieved, assigned to the

wagging mode of CH_2 groups of the surface modifier, and a significant relative intensity was obtained for the Si-F stretching mode. On the other hand, the silica structure of the bulk particles has approximately the same proportion of four- and six-membered siloxane rings, with a slight increase of the latter by *post-synthesis* fluorination, possibly due to breaking of some siloxane bridges in the more tensioned four-fold rings upon fluorination. As a result, a larger proportion of dangling Si-O bonds appears, responsible for the increase in the relative intensity of the $\nu\text{Si-OH/O}^-$ band (from 6.4 to 8.4%).

In summary, we have demonstrated that HF may act not only as catalyst of the sol-gel processes but also as fluorinating agent, enabling the synthesis of fluorinated hollow silica nanoparticles by a simple, inexpensive and safer method compared to others. This approach is an unusual and significant step towards replacement of harmful fluorination methods and expensive precursors. Although most of these particles remain aggregated in deionised water due to the high affinity of functional groups on their surface, a three-dimensional morphology prevails. A successful use of HF as *post-synthesis* fluorinating agent of bulk silica nanoparticles was also demonstrated. The outgoing nanocapsules may be potentially used for high loading drug transport and delivery, and simultaneously for ^{19}F MRI tracking. In fact, contrarily to the perfluorocarbon compounds (PFCs), these highly fluorinated silica nanoparticles are chemically stable, biologically innocuous and water soluble; besides, the size of individual particles (below 100 nm) is adequate for intracellular labels, whereas the aggregates may be useful as blood pool agents.^[29,30]

Notes and references

^a CQFM - Centro de Química-Física Molecular and IN - Institute of Nanoscience and Nanotechnology, Instituto Superior Técnico, Universidade de Lisboa, Av. Rovisco Pais 1, 1049-001 Lisboa, Portugal.

† Corresponding Author: Tel: +351-218419220, Fax: +351-218464455, e-mail: lilharco@ist.utl.pt

Luis Manuel Figueiredo Lopes acknowledges Fundação para a Ciência e a Tecnologia (FCT) for financial support (PhD grant BD/62616/2009).

Electronic Supplementary Information (ESI) available: Materials and synthesis procedures as well as the characterization techniques are included. Table S1 contains the assignments of the DRIFT spectra of all the synthesized silica nanoparticles. See DOI: 10.1039/c000000x/.

- 1 A. Tressaud, G. Haufe (eds), Fluorine and Health: Molecular Imaging, Biomedical Materials and Pharmaceuticals, Elsevier: Hungary, 2008.
- 2 R. Berger, G. Resnati, P. Metrangolo, E. Weber and J. Hulliger, *Chem. Soc. Rev.*, 2011, **40**, 3496.
- 3 J. G. Riess and M. P. Krafft, *Biomaterials*, 1998, **19**, 1529.
- 4 J. G. Riess, *Curr. Opin. Colloid Interface Sci.*, 2009, **14**, 294.
- 5 M. M. Bailey, C. M. Mahoney, K. E. Dempah, J. M. Davis, M. L. Becker, S. Khondee, E. J. Munson and C. Berkland, *Macromol. Rapid Commun.*, 2010, **31**, 87.
- 6 B. D. Ratner, A. S. Hoffman, F. J. Schoen and J. E. Lemons, *Biomaterials Science: An Introduction to Materials in Medicine*, 3rd edition, Academic Press: Canada, 2013.
- 7 H. B. Na, I. C. Song and T. Hyeon, *Adv. Mater.*, 2009, **21**, 2133.
- 8 M. Srinivas, P. A. Morel, L. A. Ernst, D. H. Laidlaw and E. T. Ahrens, *Magn. Reson. Med.*, 2007, **58**, 725.
- 9 K. Tanaka, N. Kitamura, K. Nakab and Y. Chujo, *Chem. Commun.*, 2008, 6176.
- 10 R. Schirmacher, C. Wängler and E. Schirmacher, *Mini-Reviews in Organic Chemistry*, 2007, **4**, 317.

- ¹¹ G. E. Smith, H. L. Sladen, S. C. G. Biagini and P. J. Blower, *Dalton Trans.*, 2011, **40**, 6196.
- ¹² M. J. Goette, A. H. Schmieder, T. A. Williams, J. S. Allen, J. K. Keupp, G. M. Lanza, S. A. Wickline and S. D. Caruthers, *J. Cardiovascular Magnetic Resonance*, 2013, **15** (Suppl1):O83.
- ¹³ J. L. Vivero-Escoto, R. C. Huxford-Phillips and W. Lin, *Chem. Soc. Rev.*, 2012, **41**, 2673.
- ¹⁴ E. B. Gyenge, X. Darphin, A. Wirth, U. Pieleles, H. Walt, M. Bredell and C. Maake, *J. Nanobiotech.*, 2011, **9**: 32 (14 pages).
- ¹⁵ H. Sawada, A. Sasaki, K. Sasazawa, K.-I. Toriba, H. Kakehi, M. Miura and N. Isu, *Polym. Adv. Technol.*, 2008, **19**, 419.
- ¹⁶ F. Pardal, V. Lapinte and J.-J. Robin, *J. Polym. Sci. Part A: Polym. Chem.*, 2009, **47**, 4617.
- ¹⁷ Y.-C. Sheen, Y.-C. Huang, C.-S. Liao, H.-Y. Chou and F.-C. Chang, *J. Polym. Sci. Part B: Polym. Phys.*, 2008, **46**, 1984.
- ¹⁸ X. Cui, S. Zhong, J. Yan, C. Wang, H. Zhang and H. Wang, *Colloids Surf. A*, 2010, **360**, 41.
- ¹⁹ H. Sawada, T. Narumi, A. Kajiwara, K. Ueno and K. Hamazaki, *Colloid Polym. Sci.*, 2006, **284**, 551.
- ²⁰ E. Lataste, A. Demourgues, H. Leclerc, J.-M. Goupil, A. Vimont, E. Durand, C. Labrugère, H. Benalla and A. Tressaud, *J. Phys. Chem. C*, 2008, **112**, 10943.
- ²¹ L. M. F. Lopes, M. N. Kopylovich, A. L. Pombeiro and L. M. Ilharco, *J. Phys. Chem. B*, 2012, **116**, 1189.
- ²² G. Hartmeyer, C. Marichal, B. Lebeau, P. Caullet and J. Hernandez, *J. Phys. Chem. C*, 2007, **111**, 6634.
- ²³ G. Hartmeyer, C. Marichal, B. Lebeau, S. Rigolet, P. Caullet and J. Hernandez, *J. Phys. Chem. C*, 2007, **111**, 9066.
- ²⁴ W. Coburn and M. Chen, *J. Appl. Phys.*, 1980, **51**, 3134.
- ²⁵ R. E. Youngman and S. Sen, *J. Non-Cryst. Solids*, 2004, **349**, 10.
- ²⁶ M. Yoshimaru, S. Koizumi and K. Shimokawa, *J. Vac. Sci. Technol. A*, 1997, **15**, 2915.
- ²⁷ L. Song, X. Ge, M. Wang and Z. Zhang, *J. Non-Cryst. Solids*, 2006, **352**, 2230.
- ²⁸ A. Fidalgo and L. M. Ilharco, *Chem. Eur. J.*, 2004, **10**, 392.
- ²⁹ M. Srinivas, A. Heerschap, E. T. Ahrens, C. G. Figdor and I. J. M. de Vries, *Trends Biotechnol.*, 2010, **28**, 363.
- ³⁰ Y. B. Yu, *WIREs Nanomed. Nanobiotechnol.*, 2013, **5**, 646.